Materials Advances

ROYAL SOCIETY OF CHEMISTRY

PAPER

View Article Online
View Journal | View Issue

Cite this: *Mater. Adv.*, 2023, 4, 215

Improved electrical conductivity of Co(II) and Cu(II) ladder polymers in the fabrication of photoresponsive Schottky devices†

Basudeb Dutta, ‡[ab] Dhananjoy Das,‡[c] Kumari Raksha,[a] Chittaranjan Sinha,[d] Sumit Khanra,*[a] Partha Pratim Ray[c] and Mohammad Hedayetullah Mir*[b]

Received 19th September 2022,
Accepted 9th November 2022

DOI: 10.1039/d2ma00911k

rsc.li/materials-advances

In this work, two new Cu(II) and Co(II) based coordination polymers (CPs), $[Co_2(bpd)_2(nac)_2]\cdot 2CH_3OH\cdot H_2O$ (**Co-CP**) and $[Cu_2(bpd)_2(nac)_2]\cdot 2CH_3CN\cdot 2H_2O$ (**Cu-CP**) respectively, have been synthesized using a bidentate pyridyl ligand, *N*,*N*′-bis(1-pyridine-4-yl-ethylidene) (bpd), linker with the less explored 3-(1-naphthyl)acrylic acid (nac) ligand appended at the metal centre to fulfil the molecular geometry. Here, **Co-CP** forms a one-dimensional (1D) ladder polymer, whereas **Cu-CP** consists of a combination of 1D chains and 1D ladder polymers. Interestingly, both the CPs exhibit semiconducting behaviour with increased conductivity upon illumination, signifying the photosensitive nature. However, **Cu-CP** reveals better conductivity as compared to **Co-CP**. This is obvious from the field emission electron microscopy (FESEM) study, where **Cu-CP** with flower-like morphology shows a higher surface area with respect to the rod-shaped morphology of **Co-CP**, resulting in higher charge transport. To the best of our knowledge, Co/Cu based CPs showing photosensitivity seem to be scarce. Thus, this study opens a new avenue in the fabrication of photoresponsive electronic devices.

Introduction

The dramatic revolution of laboratory to land applications of materials chemistry propagates at an extraordinary pace. Application of materials has directly been governed by the structural architecture and morphology. In this regard, coordination polymers (CPs)[1–9] have attracted materials researchers mostly because of their unique molecular structures and excellent stabilities. These hybrid molecular systems are constructed through inorganic metal ions or metal clusters and organic ligands.[10–15] Hence, the molecular properties as well as applications are also regulated by the nature of the metal centers and ligands. A combination of organic components (O-donor and N-donor ligands) is commonly exploited to achieve structural varieties and desired molecular properties.[16–18] In these coordination systems, metal salts or organic linkers are judiciously selected to confer the application field. In fact, there is an essential relationship between the structural architecture, properties and utilities of the materials. Rational construction and scientific judgment during the engineering of these crystalline materials make them easier to characterize and illustrate important structure–property relationships. In the construction of higher dimensional supramolecular architecture, various supramolecular interactions such as hydrogen bonding, π···π, C–H···π, cation···π, anion···π, halogen···halogen, halogen···π and van der Waals interactions play the crucial role.[19–21] Sometimes, these self-assembled structures are entirely unlike and more proficient than the unassembled forms. The discussed inorganic–organic hybrid materials are extremely applicable in the territory of gas sorption, molecular storage and separation, ion exchange, electrochemical catalysis, energy technology, drug delivery, temperature-dependent magnetism, sensing and detection of noxious ions and emerging analytes, proton conductance, electrical conductivity, electronic device fabrication, *etc.*[22–34]

Of these, utilization of CPs in electrical conductivity and device fabrication is particularly important as these CPs can be explored to overcome the energy crisis situation and for technological interest. However, in CPs, the poor extended electronic coupling among the metal nodes and the ligands impedes competent charge transport.[35–38] The consequential electronic

[a] *Department of Chemical Sciences, Indian Institute of Science Education and Research Kolkata, Mohanpur, West Bengal 741246, India. E-mail: sumit.khanra@iiserkol.ac.in*
[b] *Department of Chemistry, Aliah University, New Town, Kolkata 700 156, India. E-mail: chmmir@gmail.com*
[c] *Department of Physics, Jadavpur University, Jadavpur, Kolkata 700 032, India*
[d] *Department of Chemistry, Jadavpur University, Jadavpur, Kolkata 700 032, India*

† Electronic supplementary information (ESI) available: Experimental section, Tables S1–S5, Fig. S1–S12, Scheme S1 and X-ray crystallographic data in CIF format for compounds **Co-CP** and **Cu-CP**. CCDC 2203412 (**Co-CP**) and 2203413 (**Cu-CP**). For ESI and crystallographic data in CIF or other electronic format see DOI: https://doi.org/10.1039/d2ma00911k

‡ These authors contributed equally.

bands display nominal dispersion, which indicates that the electrons are strongly localized over the whole lattice. The band dispersion determines the efficacy of the compound to transmit electrical current. Therefore, the crucial facet is to adjust the electronic connection among the metal centers and the organic ligands to enhance delocalization for higher conductivity.[39–41] In this regard, a substantive number of CPs based on d^{10} metal ions (Zn^{2+}/Cd^{2+}) have been reported and those behave as semiconducting materials. Some of the materials have also exhibited photosensitivity properties, *i.e.* enhancement of conductivity upon illumination.[37] However, varying metal ions in tailor-fit synthesis, we can easily regulate the semiconducting nature as well as the photosensitivity behavior of CPs. In this facet, CPs based on Co(II)/Cu(II) metal ions with semiconducting properties have not been much explored and remain more elusive in regard to photosensitivity.[8,40]

Herein, we report two Co(II) and Cu(II) based one-dimensional (1D) CPs $[Co_2(bpd)_2(nac)_2]\cdot 2CH_3OH\cdot H_2O$ (**Co-CP**) and $[Cu_2(bpd)_2(nac)_2]\cdot 2CH_3CN\cdot 2H_2O$ (**Cu-CP**) which have been utilized to fabricate metal–semiconductor (MS) junction Schottky devices (SDs). The current–voltage (*I–V*) characteristics of the fabricated SDs were measured to estimate the diode parameters, such as on/off ratio, photosensitivity, ideality factor, barrier height, and series resistance. The study reveals that both the CPs exhibit higher charge conduction upon illumination signifying the photosensitive nature. The charge transport parameters including mobility and lifetime of the charge carriers were also investigated with the help of the space–charge limited current (SCLC) theory, which demonstrates the improved device performance of **Co-CP** and **Cu-CP**. However, **Cu-CP** exhibits better conductivity with respect to **Co-CP**. This observation is also supported by a field emission scanning electron microscope (FESEM) study. Flower-like morphology of **Cu-CP** offers higher surface area as compared to rod-shaped **Co-CP** and exhibits increased electrical conductivity.

Results and discussion

Structural description of $[Co_2(bpd)_2(nac)_2]\cdot 2CH_3OH\cdot H_2O$ (Co-CP)

The single crystal X-ray diffraction (SCXRD) study reveals that **Co-CP** crystallizes in the monoclinic space group *C*2/*c*. The asymmetric unit consists of one Co(II) centre, two nac ligands and a bpd ligand. The asymmetric unit further contains one each of CH_3OH and H_2O molecules in the lattice (Fig. S1, ESI†). The Co(II) centre adopts a six-coordinated octahedral geometry (Fig. 1). The equatorial plane is defined by two O atoms of a chelating nac ligand and two O atoms of two bridging nac ligands. To complete the octahedron, two N atoms from two bpd ligands take the axial positions. Here also, two Co(II) centres and two bridging carboxylate groups form a dinuclear 8-membered $[Cu_2(O_2CC)_2]$ secondary building unit (SBU) with Co···Co distance of 4.3064 Å. Thereby, a pair of bpd ligands are aligned parallel *via* π···π stacking contacts with the centroid–centroid distance of 3.986 Å (Fig. 1). A crystallographic inversion centre is also found in the middle of the ring. The SBUs

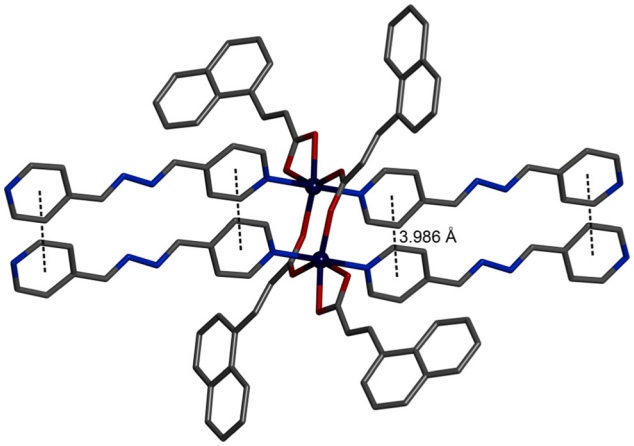

Fig. 1 Dimeric SBU of **Co-CP** with coordination environment around Co(II) centres. Carbon: gray; nitrogen: blue; oxygen: red; cobalt: navy. Hydrogen atoms and solvent molecules are not shown for clarity. Dashed lines represent the π···π contacts between bpd ligands.

and a pair of bpd ligands are combined to generate a 1D ladder polymer. Further, the 1D ladder polymers undergo extensive π···π stacking interactions with the centroid–centroid distance of 3.766–3.849 Å to form a 3D supramolecular assembly. In the solid-state structure, if the π···π interactions are considered as joining the ladder polymers, they would generate a 2D layer structure. The aligned bpd pairs act as pillars which join the 2D layers into a doubly interpenetrated 3D supramolecular pillar-layered network of cubic topology (Fig. 2 and Fig. S2, ESI†).

Structural description of $[Cu_2(bpd)_2(nac)_2]\cdot 2CH_3CN\cdot 2H_2O$ (Cu-CP)

The SCXRD study reveals that **Cu-CP** also crystallizes in the monoclinic space group *C*2/*c*. The asymmetric unit contains two parts (Fig. S3, ESI†). The first part consists of a Cu(II) centre (Cu1), one bpd ligand and two nac ligands. However, the second part comprises a Cu(II) centre (Cu2), half a bpd ligand and one nac ligand. The asymmetric unit further consists of

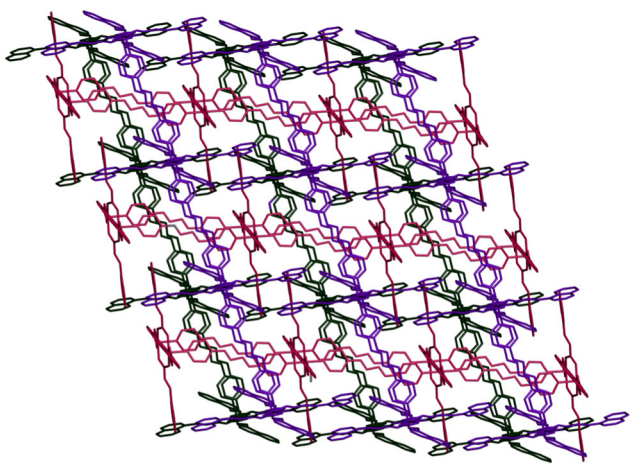

Fig. 2 Doubly interpenetrated 3D supramolecular pillar-layered structure of **Co-CP**.

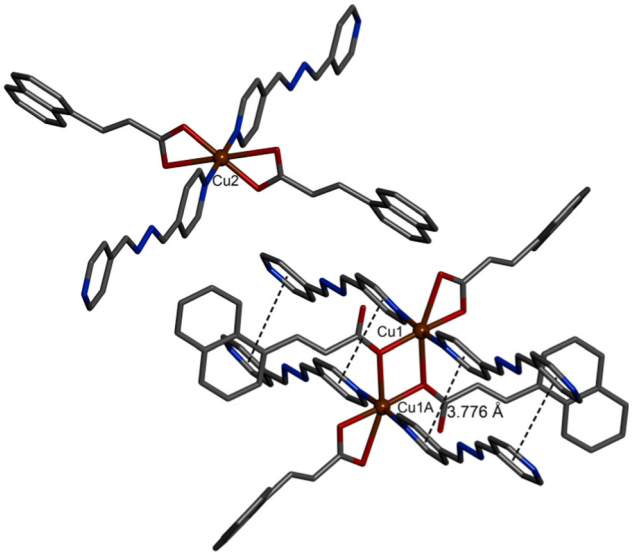

Fig. 3 Coordination environment around Cu(II) centres of **Cu-CP**. Carbon: gray; nitrogen: blue; oxygen: red; copper: brown. Hydrogen atoms and solvent molecules are not shown for clarity. Dashed lines represent the π···π stacking interactions between bpd ligands.

one each of CH_3CN and H_2O molecules in the lattice (Fig. S3, ESI†). All the Cu(II) centres adopt six-coordinated octahedral geometries (Fig. 3). The equatorial plane of the octahedron is formed by two O atoms from a chelating nac ligand and two O atoms from two nac ligands. Two N atoms of two bpd ligands occupy the axial positions. Here, two Cu(II) centres and bridging carboxylate groups form a 8-membered dinuclear $[Cu_2(O_2CC)_2]$ secondary building unit (SBU) with Cu···Cu distance of 3.4843(6) Å. A pair of bpd ligands are aligned *via* face-to-face π···π stacking interactions (centroid–centroid distance 3.776 Å) (Fig. 3). A crystallographic inversion centre is present in the middle of the $[Cu_2(O_2CC)_2]$ ring. A 1D ladder polymer is obtained by the combination of SBUs and a pair of bpd ligands (Fig. 4).

On the other hand, the Cu2 centre is surrounded by four O atoms of two carboxylate groups from two individual chelating nac ligands forming the equatorial plane, while two N atoms from two individual bpd ligands complete the octahedral geometry. The connectivity of the Cu2 centre and nac ligand leads to the formation of a 1D linear chain. Further, 1D ladder polymers and 1D linear chains are assembled to form 3D supramolecular frameworks by the arrangement of extensive face-to-face π···π stacking interactions (centroid–centroid distance 3.834 Å), and C–H···π interactions with edge-to-face distance of 3.023–3.160 Å (Fig. 4 and Fig. S4, ESI†).

Surface morphological studies

The surface morphologies of the **Co-CP** and **Cu-CP** were investigated using FESEM micrographs and are displayed in Fig. 5 and 6. These kinds of microstructures of the polymers not only help to study shapes and sizes, but also show the characteristics of the MS junction that is formed while fabricating the Schottky diodes. It is observed from the images that the **Co-CP** are rod-shaped (Fig. 5), while the **Cu-CP** are flower-like (Fig. 6). The flower-like shapes offer higher surface area, contributing to the higher contact area and larger electrical conduction.[42] This study prompts us to investigate further the electrical conductivity of the materials.

Optical properties

The optical spectra of **Co-CP** and **Cu-CP** were recorded to estimate their optical band gaps. To deduce the band gaps, Tauc's equation (eqn (1))[43] was employed, which is given by:

$$(\alpha h\nu)^n = A(h\nu - E_g) \quad (1)$$

where α is the absorption coefficient, E_g is the bandgap, h is Planck's constant, ν is frequency, A is a constant, and $n = 2$ and 1/2 corresponding to the allowed direct and indirect optical transitions, respectively. By extrapolating the linear region of the plot $(\alpha h\nu)^2$ *vs.* $h\nu$ to $\alpha = 0$, as displayed in Fig. S11 (ESI†), the direct optical band gaps of **Co-CP** and **Cu-CP** were evaluated as 3.48 eV and 3.46 eV respectively, which suggest the intermediate band gap region.[31]

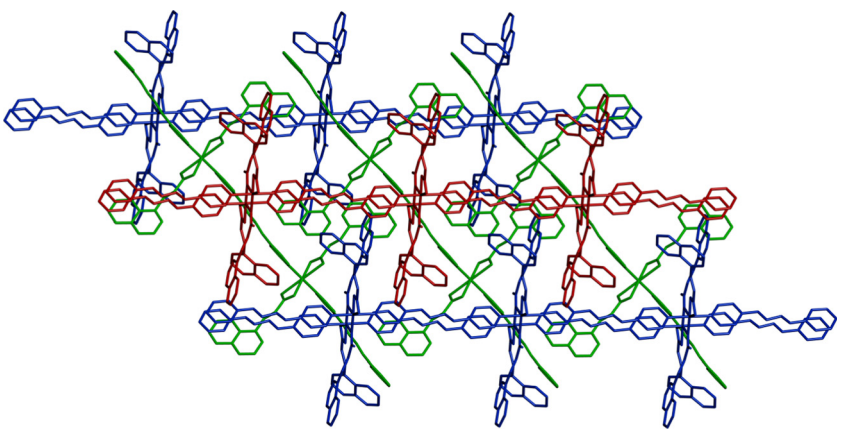

Fig. 4 The 3D supramolecular network of **Cu-CP** comprising 1D ladder polymers and 1D linear chains.

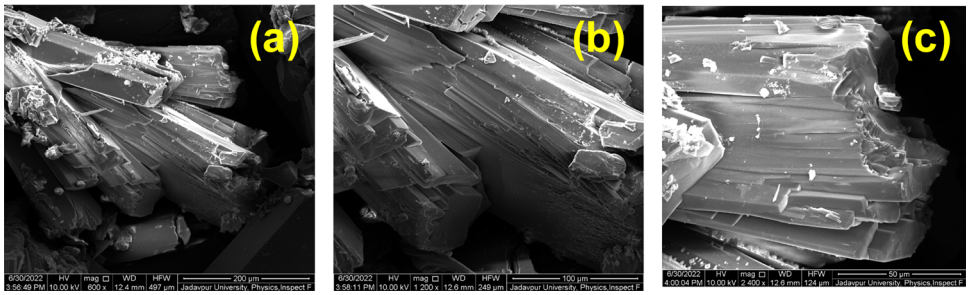

Fig. 5 FESEM micrographs of **Co-CP**.

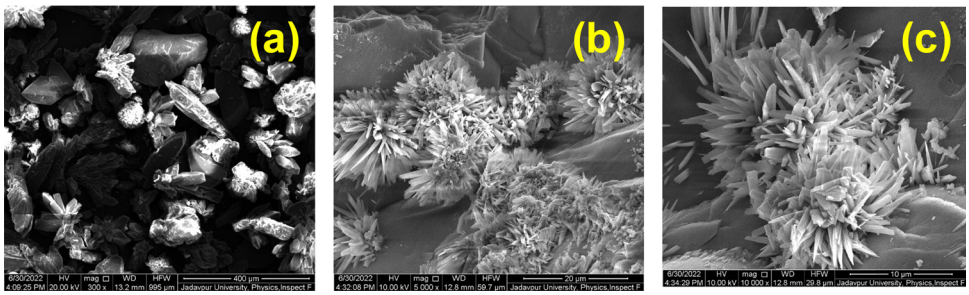

Fig. 6 FESEM micrographs of **Cu-CP**.

Device fabrication method

To study the electrical characteristics of **Co-CP** and **Cu-CP**, the MS junction SDs based on these CPs were fabricated. In a typical method, first ITO-coated glass substrates were cleaned using acetone, followed by 2-propanol and distilled water. Then, on the top of the cleaned indium tin oxide (ITO) coated substrate, a thin film of **Co-CP**/**Cu-CP** was deposited by the spin coating unit. Subsequently, the as-prepared films were dried in a vacuum oven for 1 h. Next, as a metallic contact, aluminium (Al) was deposited onto the coated film using a vacuum coating unit (12A4D, HINDHIVAC) under an atmospheric pressure of 4.7×10^{-6} torr in the deposition method. In this process, a typical quad punch-hole shadow mask was used to control the effective diode area of the Schottky device as 7.065×10^{-6} m^{-2}. The schematic diagram of the Al/CPs/ITO structure is portrayed in Scheme 1.

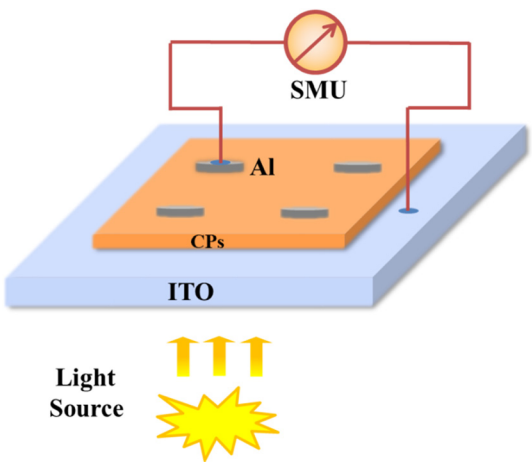

Scheme 1 Schematic diagram of the fabricated Al/CPs/ITO SDs.

Current–voltage (*I*–*V*) measurement

The electrical properties of the MS junction thin-film devices of **Co-CP** and **Cu-CP** were investigated. For this, the current–voltage (*I*–*V*) characteristics of the CP based Schottky devices were studied between the applied bias voltage of ±1 V under dark and light conditions. The *I*–*V* characteristics of the ITO/CPs/Al configurations presented in Fig. 7 exhibit a nonlinear rectifying behaviour for the SDs. The conductivities of the CPs under dark and light conditions were measured. It has been observed that the charge conduction is higher under illumination for both of the CPs, signifying the photo-responsive nature.

The current *vs.* voltage characteristics of the CP-based SDs were further discussed using thermionic emission (TE) theory.[44] Here, the differential method first exploited by Cheung *et al.* was employed to evaluate different SD parameters.[45] The current density (J) *vs.* voltage (V) curves could be written as:[46]

$$J = J_S\left[\exp\left(\frac{qV_D}{\eta kT}\right) - 1\right] \quad (2)$$

where q is the charge of the electron, k is the Boltzmann constant, T is the temperature, V_D is the potential drop and η is the ideality factor J and J_S are respectively the current density and the current density at saturation, which is also given by:

$$J_S = A^* T^2 \exp\left(\frac{-q\phi_B}{kT}\right) \quad (3)$$

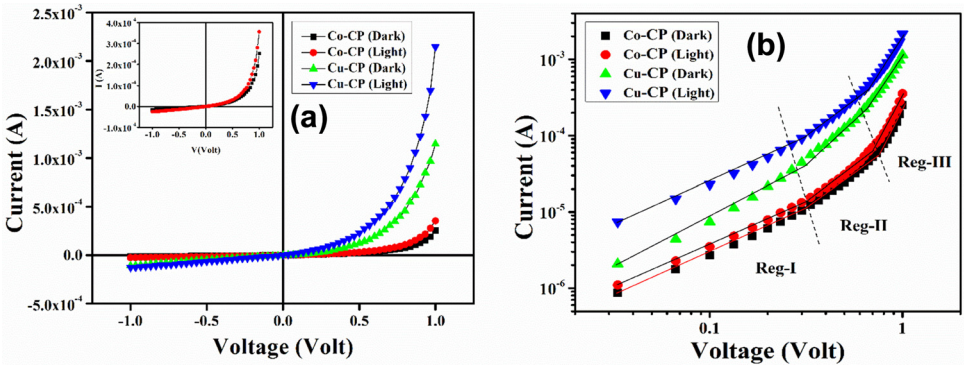

Fig. 7 (a) *I*–*V* characteristics curves for **Co-CP** and **Cu-CP** based devices. (b) *I*–*V* curves on logarithmic scale.

where A^* stands for the Richardson constant and ϕ_B is the barrier height. Considering $V_D = V - IR_S$ using the Cheung and Cheung method,[47] eqn (2) could be reduced to the following differential form:

$$G(J) = \frac{dV}{d(\ln J)} = \left(\frac{\eta kT}{q}\right) + A_{eff} R_S J \quad (4)$$

Furthermore, considering the function $H(J)$ as eqn (5), the barrier or potential height of the SDs was deduced using the following eqn (6):

$$H(J) = V - \left(\frac{\eta kT}{q}\right) \ln\left(\frac{J}{A^* T^2}\right) \quad (5)$$

$$H(J) = A_{eff} R_S J + \eta \phi_B \quad (6)$$

The $G(J)$ *vs.* J and $H(J)$ *vs.* J graphs for dark and light conditions are presented in Fig. 8(a–d) respectively. The ideality factor (η) and series resistance (R_S) were determined from the intercept

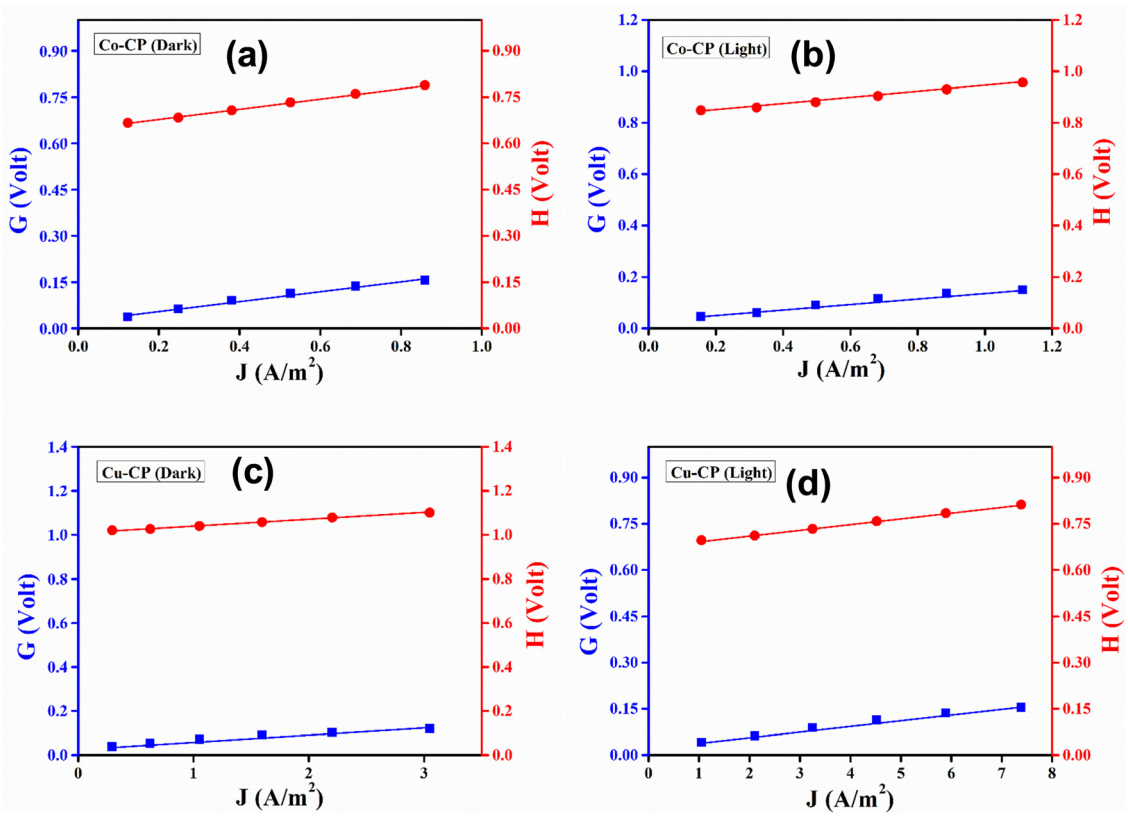

Fig. 8 *G vs. J* and *H vs. J* plots under dark and light conditions for (a and b) **Co-CP**, and (c and d) **Cu-CP** based thin-film devices.

Table 1 Charge transport parameters

	Photosensitivity (S)	Conductivity (σ) (S m^{-1})	
		Dark	Light
Co-CP	0.41	4.78×10^{-6}	6.15×10^{-6}
Cu-CP	0.86	19.97×10^{-6}	70.61×10^{-6}

Table 2 Schottky diode parameters

	Ideality factor (η)		Barrier height (ϕ_B) (eV)		Series resistance (R_S) (kΩ)	
	Dark	Light	Dark	Light	Dark	Light
Co-CP	0.89	1.15	0.72	0.71	23.42	16.41
Cu-CP	1.43	1.01	0.70	0.66	4.21	2.60

and slope of the linearly fitted plot of G *vs.* J, respectively. On the other hand, the barrier heights (ϕ_B) for the **Co-CP** and **Cu-CP** based devices are determined from the H *vs.* J plot. The obtained values of the photosensitivity and the dc conductivity under dark and illumination conditions are listed in Table 1, which depicts that **Cu-CP** is more photo responsive than **Co-CP**. Also, **Cu-CP** exhibits higher conductivity as compared to **Co-CP**.

The measured ideality factors (η), series resistances (R_S) and barrier heights (ϕ_B) for **Co-CP** and **Cu-CP** under both dark and illumination conditions are listed in Table 2. It is observed that, after light soaking, the ideality factor of both of the CP-based devices approached very close to 1, indicating a more ideal device. This is generally due to the reduced photo-carrier recombination at the junction under light irradiation.[43] In the presence of light, the series resistances were drastically reduced compared to the dark condition, causing a large increase in the photocurrent. The evaluated values of barrier height also show that under light, the turn-on voltages were slightly decreased. Table 2 manifests the improved diode behaviour for the **Cu-CP** based diodes. Also, the enhanced performance of both of the devices after light illumination portrays the excellent potential of **Co-CP** and **Cu-CP** in the field of various optoelectronic devices.

The study of different diode parameters led us to thoroughly observe the charge transport properties of the CPs. In this regard, the I–V curves are plotted on the logarithmic scale (Fig. 7b). Fig. 7b reveals three distinguishable slopes, which are marked as region-I, II and III. In region-I, the current follows as $I \propto V$, which denotes the ohmic region. In the second region, the slope is close to 2, where the current varies as $I \propto V^2$ and is controlled by the space–charge limited current (SCLC) field (Fig. 9).[48] The injected carriers increase much higher as proportional to the background carriers. As a result, it spreads all over the space and creates a space–charge field. In region III, the injection level of electrons is much higher and they follow the power-law ($I \propto V^n$, where $n > 2$).

Following this model, the effective carrier mobility was deduced using the Mott–Gurney equation:[49]

$$I = \frac{9\mu_{\text{eff}}\varepsilon_0\varepsilon_r A_{\text{eff}}}{8}\left(\frac{V^2}{d^3}\right) \quad (7)$$

where A_{eff}, ε_0, ε_r and d are the effective diode area, the free space permittivity, the dielectric constant of the materials and the thickness of the diode, respectively. The dielectric constant (ε_r) was evaluated from the capacitance *vs.* frequency plot (Fig. 10) by employing the following equation:[50]

$$\varepsilon_r = \frac{Cd}{\varepsilon_0 A} \quad (8)$$

where C is the capacitance at saturation, d is the thickness of the film, A is the effective area and ε_0 is the permittivity of free space.

Transit time (τ), which is another key parameter to study charge transport across the SD junction,[51] was evaluated using the following equation:

$$\tau = \frac{9\varepsilon_0\varepsilon_r A_{\text{eff}}}{8d}\left(\frac{V}{I}\right) \quad (9)$$

All the deduced values of the diode parameters displayed that the charge conduction of the CPs was improved after light irradiation (Table 3). Also, the higher conductivity (Table 1) of **Cu-CP** could be accredited to its higher mobility and lower transit or lifetime. It is also to be noted that the diode characteristics as well as the transport parameters of both the Co(II) and Cu(II) CP based SDs demonstrate much enhanced charge transfer properties after light soaking (Scheme S1, ESI†). The transient photocurrent *vs.* time measurements were performed to study the conducting mechanism of the CPs. It is

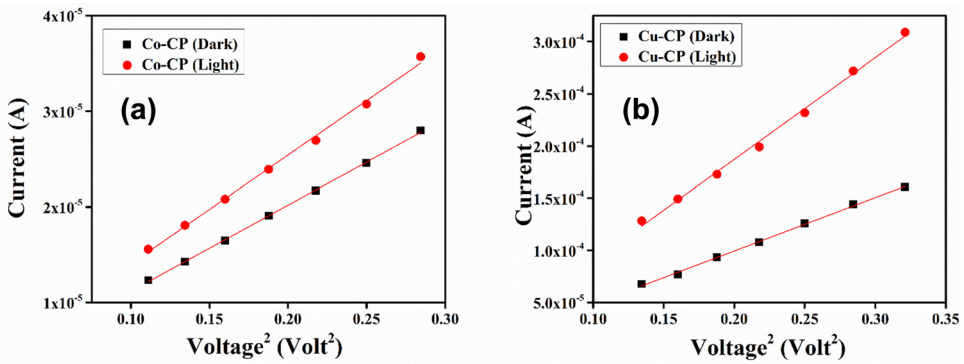

Fig. 9 I *vs.* V^2 curves under both dark and light conditions for (a) **Co-CP** and (b) **Cu-CP** based thin-film devices.

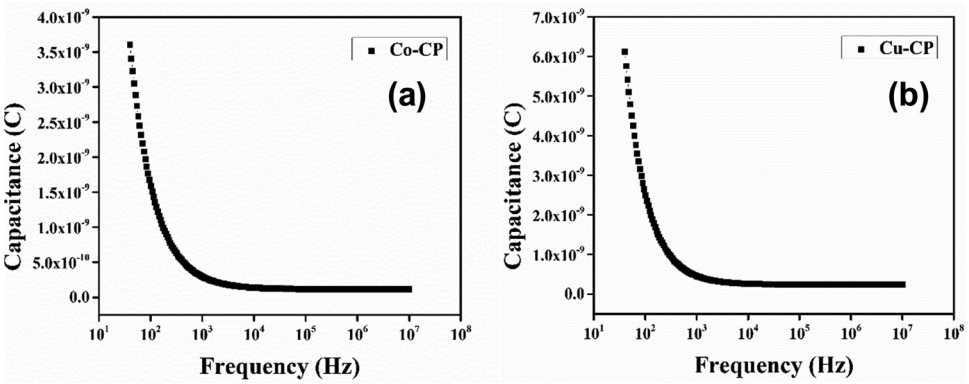

Fig. 10 Capacitance *versus* frequency (*C*–*f*) plots of (a) **Co-CP** and (b) **Cu-CP**.

Table 3 SCLC parameters

		μ_{eff} ($m^2\ V^{-1}\ s^{-1}$)		τ (s)	
	ε_r	Dark	Light	Dark	Light
Co-CP	1.15×10^{-10}	6.94×10^{-7}	8.72×10^{-7}	1.66×10^{-6}	1.31×10^{-6}
Cu-CP	2.34×10^{-10}	1.94×10^{-6}	3.70×10^{-6}	5.51×10^{-7}	2.90×10^{-7}

observed that the conductivity of the CP does not vary with the passage of time (Fig. S12, ESI†). Thus, **Co-CP** and **Cu-CP** display immense potential to be employed in photoresponsive device applications.

Conclusion

In summary, the present work analyses an unusual utilization of transition metal ions in the fabrication of CPs. Here, less explored nac acts as an ancillary ligand and bpd links the metal centres to generate 1D chains. The materials have been employed to fabricate semiconducting Schottky devices; through which electrical properties have been analyzed. Interestingly, the electrical conductivities of the materials have been enhanced upon light illumination. Therefore, the synthesized CPs can act as next generation photosensitive electronic materials. Charge transportation and electrical conductivity are also well tuned with the metal nodes present in the structural architecture. This work can be an inspiration for future researchers in the field of materials science.

Conflicts of interest

There are no conflicts to declare.

Acknowledgements

This work was supported by UGC-DAE CSR, India (Grant No. CRS/2021-22/02/538 Dated 30/03/2022). B. D. thanks the Indian Institute of Science Education and Research Kolkata for IISER-K PDF fellowship. P. P. R. gratefully acknowledges the financial support of this work by SERB-DST, Govt. of India (Sanction No. EMR/2016/005387, Dated – 24.07.2017). All the authors thank Jadavpur University, Kolkata, India for the instrumental facility.

References

1 S. R. Batten, S. M. Neville and D. R. Turner, *Coordination Polymers: Design, Analysis and Application*, Royal Society of Chemistry, Cambridge, 2009.
2 H.-C. Zhou and S. Kitagawa, *Chem. Soc. Rev.*, 2014, **43**, 5415–5418.
3 S. Halder, A. Dey, A. Bhattacharjee, J. Ortega-Castro, A. Frontera, P. P. Ray and P. Roy, *Dalton Trans.*, 2017, **46**, 11239–11249.
4 J. Duan, W. Jin and S. Kitagawa, *Chem. Soc. Rev.*, 2017, **332**, 48–74.
5 D. Sun, S. Yuan, H. Wang, H.-F. Lu, S.-Y. Feng and D.-F. Sun, *Chem. Commun.*, 2013, **49**, 6152–6154.
6 S. S. Kumar, N. Kurra and H. N. Alshareef, *J. Mater. Chem. C*, 2016, **4**, 215–221.
7 D. Cardenas-Morcoso, E. Vey, M. Heiderscheid, G. Frache and N. D. Boscher, *J. Mater. Chem. C*, 2022, **10**, 2194–2204.
8 F. Ahmed, S. Halder, B. Dutta, S. Islam, C. Sen, S. Kundu, C. Sinha, P. P. Ray and M. H. Mir, *New J. Chem.*, 2017, **41**, 11317–11323.
9 B. Dutta, A. Dey, C. Sinha, P. P. Ray and M. H. Mir, *Inorg. Chem.*, 2019, **58**, 5419–5422.
10 T. Panda and R. Banerjee, *Proc. Natl. Acad. Sci., India, Sect. A*, 2014, **84**, 331–336.
11 K. Naskar, S. Sil, N. Sahu, B. Dutta, A. M. Z. Slawin, P. P. Ray and C. Sinha, *Cryst. Growth Des.*, 2019, **19**, 2632–2641.
12 F. Ahmed, S. R. Ghosh, S. Halder, S. Guin, S. M. Alam, P. P. Ray, A. D. Jana and M. H. Mir, *New J. Chem.*, 2019, **43**, 2710–2717.

13 J. J. Vittal, *Coord. Chem. Rev.*, 2007, **251**, 1781–1795.
14 M. Dincă and J. R. Long, *J. Am. Chem. Soc.*, 2005, **127**, 9376–9377.
15 B. Dutta, A. Dey, K. Naskar, S. Maity, F. Ahmed, S. Islam, C. Sinha, P. Ghosh, P. P. Ray and M. H. Mir, *New J. Chem.*, 2018, **42**, 10309–10316.
16 A. A. Talin, A. Centrone, A. C. Ford, M. E. Foster, V. Stavila, P. Haney, R. A. Kinney, V. Szalai, F. El Gabaly, H. P. Yoon, F. Leonard and M. D. Allendorf, *Science*, 2014, **343**, 66–69.
17 B. Dutta, R. Jana, A. K. Bhanja, P. P. Ray, C. Sinha and M. H. Mir, *Inorg. Chem.*, 2019, **58**, 2686–2694.
18 T. Komatsu, J. M. Taylor and H. Kitagawa, *Inorg. Chem.*, 2016, **55**, 546–548.
19 S. Naaz, B. Debnath, S. Islam, S. Khan, F. Ahmed, B. Dutta, A. D. Jana and M. H. Mir, *Cryst. Growth Des.*, 2022, **22**, 1253–1262.
20 P. Ghorai, A. Dey, A. Hazra, B. Dutta, P. Brandão, P. P. Ray, P. Banerjee and A. Saha, *Cryst. Growth Des.*, 2019, **19**, 6431–6447.
21 F. Ahmed, B. Dutta and M. H. Mir, *Dalton Trans.*, 2021, **50**, 29–38.
22 F. B. de Almeida, M. da Silva Cunha, W. P. Barros, H. A. De Abreu and R. Diniz, *J. Phys. Chem. C*, 2020, **124**, 21103–21112.
23 M. I. Velasco, R. H. Acosta, W. A. Marmisollé, O. Azzaroni and M. Rafti, *J. Phys. Chem. C*, 2019, **123**, 21076–21082.
24 B. Dutta, R. Jana, A. K. Bhanja, P. P. Ray, C. Sinha and M. H. Mir, *Inorg. Chem.*, 2019, **58**, 2686–2694.
25 M. L. Hu, M. Abbasi-Azad, B. Habibi, F. Rouhani, H. Moghanni-Bavil-Olyaei, K. G. Liu and A. Morsali, *ChemPlusChem*, 2020, **85**, 2397–2418.
26 Y. Park, J. Jung and M. Chang, *Appl. Sci.*, 2019, **9**, 1070.
27 G. Chakraborty, I.-H. Park, R. Medishetty and J. J. Vittal, *Chem. Rev.*, 2021, **121**, 3751–3891.
28 T. A. Fernandes, I. F. Costa, P. Jorge, A. C. Sousa, V. André, N. Cerca and A. M. Kirillov, *ACS Appl. Mater. Interfaces*, 2021, **13**, 12836–12844.
29 M. Moghaddam-Manesh, D. Ghazanfari, E. Sheikhhosseini and M. Akhgar, *Appl. Organomet. Chem.*, 2020, **34**, e5543.
30 B. Dutta, R. Jana, C. Sinha, P. P. Ray and M. H. Mir, *Inorg. Chem. Front.*, 2018, **5**, 1998–2005.
31 W.-M. Chen, X.-L. Meng, G.-L. Zhuang, Z. Wang, M. Kurmoo, Q.-Q. Zhao, X.-P. Wang, B. Shan, C.-H. Tung and D. Sun, *J. Mater. Chem. A*, 2017, **5**, 13079–13085.
32 L.-L. Han, S.-N. Wang, Z. Jagličić, S.-Y. Zeng, J. Zheng, Z.-H. Li, J.-S. Chen and D. Sun, *CrystEngComm*, 2015, **17**, 1405–1415.
33 X. Gao, S.-S. Zhang, H. Yan, Y.-W. Li, Q.-Y. Liu, X.-P. Wang, C.-H. Tung, H.-Y. Ma and D. Sun, *CrystEngComm*, 2018, **20**, 4905–4909.
34 X.-P. Wang, Y.-Q. Zhao, Z. Jagličić, S.-N. Wang, S.-J. Lin, X.-Y. Li and D. Sun, *Dalton Trans.*, 2015, **44**, 11013–11020.
35 B. Dutta, A. Dey, S. Maity, C. Sinha, P. P. Ray and M. H. Mir, *ACS Omega*, 2018, **3**, 12060–12067.
36 V. Stavila, A. A. Talin and M. D. Allendorf, *Chem. Soc. Rev.*, 2014, **43**, 5994–6010.
37 S. Roy, A. Dey, P. P. Ray, J. Ortega-Castro, A. Frontera and S. Chattopadhyay, *Chem. Commun.*, 2015, **51**, 12974.
38 S. Islam, J. Datta, S. Maity, B. Dutta, S. Khan, P. Ghosh, P. P. Ray and M. H. Mir, *Cryst. Growth Des.*, 2019, **19**, 4057–4062.
39 P. Amo-Ochoa, O. Castillo, S. S. Alexandre, L. Welte, P. J. de Pablo, I. Rodriguez-Tapiador, J. Gomez-Herrero and F. Zamora, *Inorg. Chem.*, 2009, **48**, 7931–7936.
40 F. Ahmed, J. Datta, S. Khan, B. Dutta, S. Islam, S. Naaz, P. P. Ray and M. H. Mir, *New J. Chem.*, 2020, **44**, 9004–9009.
41 B. Dutta, A. Dey, C. Sinha, P. P. Ray and M. H. Mir, *Dalton Trans.*, 2019, **48**, 11259–11267.
42 A. R. Padmavathi, P. Sriyutha Murthy, A. Das, P. A. Nishad, R. Pandian and T. S. Rao, *Biofouling*, 2019, **35**, 1007–1025.
43 J. Tauc, R. Grigorovici and A. Vancu, *Phys. Status Solidi B*, 1966, **15**, 627–637.
44 S. M. Sze, *Physics of Semiconductor Devices*, Wiley, New York, 2nd edn, 1981.
45 S. K. Cheung and N. W. Cheung, *Appl. Phys. Lett.*, 1986, **49**, 85–87.
46 E. H. Rhoderick and R. H. Williams, *Metal–semiconductor contacts*, Clarendon, Oxford, 2nd edn, 1988.
47 M. Das, J. Datta, R. Jana, S. Sil, S. Halder and P. P. Ray, *New J. Chem.*, 2017, **41**, 5476–5486.
48 M. Soylu and B. Abay, *Phys. E: Low-Dimens. Syst. Nanostructures*, 2010, **43**, 534–538.
49 I. Ullah, M. Shah, M. Khan and F. Wahab, *J. Electron. Mater.*, 2016, **45**, 1175–1183.
50 S. Sil, A. Dey, J. Datta, M. Das, R. Jana, S. Halder, J. Dhar, D. Sanyal and P. P. Ray, *Mater. Res. Bull.*, 2018, **106**, 337–345.
51 D. Das, M. Das, S. Sil, P. Sahu and P. P. Ray, *ACS Omega*, 2022, **7**, 26483–26494.